$Tb_xEr_{1-x}Ni_5$ compounds: An ideal model system for competing Ising-*XY* anisotropy energies

A. N. Pirogov,[1,2,*] J.-G. Park,[1,3,4,†] A. S. Ermolenko,[2] A. V. Korolev,[2] A. G. Kuchin,[2] Seongsu Lee,[1,5] Y. N. Choi,[5] Junghwan Park,[1,3] Mahipal Ranot,[1] Junghwan Yi,[1] E. G. Gerasimov,[2] Yu. A. Dorofeev,[2] A. P. Vokhmyanin,[2] A. A. Podlesnyak,[6,7] and I. P. Swainson[8]

[1]*Department of Physics, SungKyunKwan University, Suwon 440-746, Korea*

[2]*Institute of Metal Physics, Russian Academy of Sciences, S. Kovalevskya 18, 620041 Ekaterinburg, Russia*

[3]*Department of Energy Science, SungKyunKwan University, Suwon 440-746, Korea*

[4]*Center for Strongly Correlated Materials Research, Seoul National University, Seoul 151-712, Korea*

[5]*Neutron Science Division, Korea Atomic Energy Research Institute, Daejeon 305-600, Korea*

[6]*Laboratory for Neutron Scattering, ETH Zurich and Paul Scherrer Institut, CH-5232 Villigen PSI, Switzerland*

[7]*Spallation Neutron Source, Oak Ridge National Laboratory, Oak Ridge, Tennessee 37831, USA*

[8]*NRC, Chalk River Laboratories, Chalk River, Ontario, Canada K0J 1J0*

(Received 7 March 2009; published 11 May 2009)

We have studied $Tb_xEr_{1-x}Ni_5$ ($x=0$, 0.1, 0.2, 0.3, 0.4, 0.6, 0.8, 0.925, and 1.0) compounds by using several experimental techniques such as ac-susceptibility, heat-capacity, and neutron-diffraction measurements. All the compounds are found to crystallize in the $CaCu_5$-type structure with space group $P6/mmm$. The a axis shows a linear increase with Tb concentration, whereas the c axis remains almost unchanged over the whole doping range. Our neutron-diffraction studies revealed that samples for $0 \leq x \leq 0.8$ have a commensurate magnetic structure with $\mathbf{k}=0$, whereas the two samples on the Tb-rich phase ($x=0.925$ and 1.0) have an incommensurate structure. Of particular interest is that individual Tb and Er moments keep their mutually orthogonal arrangement seen at the end-member compositions over the whole doping range, due to very strong magnetic anisotropy of single-ion nature. We have established a complete magnetic x-T phase diagram of $Tb_xEr_{1-x}Ni_5$ to find that two straight lines of the ordering of the Tb and Er subsystems are persistently seen, which intersect at a tetracritical point.

DOI: 10.1103/PhysRevB.79.174412 PACS number(s): 75.30.Kz, 75.30.Gw, 75.25.+z

I. INTRODUCTION

Random magnetic systems are the subject of extensive experimental and theoretical studies over the last three decades.[1–5] Of interest are compositionally disordered alloys, especially pseudobinary rare-earth (R) 3d metal intermetallic compounds. These disordered magnetic systems often exhibit competing magnetic interactions of several origins: for example, long-range Ruderman-Kittel-Kasuya-Yoshida (RKKY) exchange coupling, a crystal-field interaction, etc. These competing interactions would then give rise to many interesting effects, e.g., canted and incommensurate magnetic structures, spin-reorientation transitions, exchange bias phenomena, first-order magnetization process, and charge-density or spin-density waves, to name only a few.[6–10]

Systems that have competing anisotropy energies are particularly interesting.[11–13] There has been recently renewed interest in such systems thanks to the latest studies of patterned recording medium with competing induced uniaxial magnetic anisotropy and a magnetocrystalline anisotropy.[14] Of several examples, two particular types of the competing systems have been mostly studied, i.e., a random mixture of the easy axis-easy axis anisotropies (Ising-Ising type)[15,16] and a mixture of the easy axis-easy plane anisotropies (Ising-*XY* type).[17–19] These crystalline mixtures have only composition disorder that makes the direction of an easy magnetic axis to depend on single-ion anisotropy at that individual site. In both cases, mean-field theories have predicted a concentration (x)-temperature (T) phase diagram with three ordered phases: two antiferromagnetic phases similar to those of the end compounds and an additional *mixed ordering* phase. Renormalization-group calculations[20,21] have also shown that four lines, separating these phases, meet at a *decoupled* tetracritical point, and an orthogonal arrangement of the spin components occurs in the *mixed ordering* phase. These theoretical predictions were indeed borne out by the experimental studies of the antiferromagnetic Ising-Ising system, $Fe_{1-x}Co_xCl_2 \cdot 2H_2O$.[22] However, in some competing Ising-*XY* systems such as $Fe_{1-x}Co_xCl_2$, the magnetic phase diagram contains only two upper lines, while the other two lower lines expected of the theories are often quite broad and difficult to resolve experimentally.[23] Besides, the neutron-diffraction studies showed that no long-range order exists associated with the lower transition, and only short-ranged correlations were observed experimentally.

The ferromagnetic Ising-*XY* system was theoretically investigated in Ref. 11 some 20 years ago, with quantitative analysis only for concentrations in the vicinity of the ideal easy-axis and easy-plane ferromagnets. Since then, several ferromagnetic alloys, e.g., $(Ho_{1-x}Er_x)Rh_4B_4$, have been studied by the neutron-diffraction technique with a conclusion of the independent orthogonal ordering of Ho- and Er-magnetic moments.[17] In comparison to our present work, however, we should point out that to the best of our knowledge a complete magnetic phase diagram of $(Ho_{1-x}Er_x)Rh_4B_4$ alloys has not been established yet.

Magnetic phase diagrams of ferromagnetic Ising-*XY* systems, including a *decoupled* tetracritical point, were also examined by Ermolenko *et al.*[24–27] By using magnetization, susceptibility, and heat-capacity measurements, they studied

$R_xR'_{1-x}Ni_5$ hexagonal alloys for $0 \leq x \leq 1$, where R (Nd and Dy) has an XY anisotropy and R' (Sm) shows an Ising anisotropy. It is noticeable that the RNi_5 compounds possess large magnetocrystalline anisotropy, arising from the crystalline electric field splitting of rare-earth ions.[28] The overall crystal-field splitting of rare-earth ions is on the order of about 300 K. By taking into account the low value—mostly below 30 K—of the Curie temperature (T_C) of RNi_5 compounds, one can infer that the magnetic anisotropy energy exceeds the exchange energy, at least, by one order of magnitude.[29] Therefore, it is quite possible that the orientation of the individual easy magnetic directions of R and R' ions could remain unperturbed by doping. This means that the independent orthogonal ordering of R and R' moments could be realized in the pseudo-binary compounds of $R_xR'_{1-x}Ni_5$. Thus, $R_xR'_{1-x}Ni_5$ is a good model system with two noninteracting order parameters. At the same time, it has been pointed out in Refs. 25–27 that even small fields can easily influence the Curie temperature and the magnetic state of such alloys. Therefore, it is essential for one to undertake neutron-diffraction studies in order to obtain a convincing proof of the existence of the *decoupled* tetracritical point in $R_xR'_{1-x}Ni_5$, which is still elusive.

In this paper, we have made comprehensive studies of hexagonal $Tb_xEr_{1-x}Ni_5$ compounds by using ac-susceptibility, magnetization heat-capacity, and neutron-diffraction measurements. $Tb_xEr_{1-x}Ni_5$ is a good experimental realization of Ising-XY anisotropies: the Tb ions exhibit a planar XY anisotropy while the Er ions possess a c-axis Ising anisotropy. Another interesting feature of $ErNi_5$ and $TbNi_5$ is that the former is a collinear ferromagnet,[30] while the latter is known to have an incommensurate magnetic structure with a large periodicity of 200 Å. Consequently, one can expect a commensurate-incommensurate transition to occur at a critical concentration in $Tb_xEr_{1-x}Ni_5$ as well.

Up to now, two competing models have been suggested of the incommensurate magnetic structure of $TbNi_5$.[31–33] In our model[31,32] (hereinafter denoted as a FAN-like model), a magnetic order is described as the superposition of a ferromagnetic moment along the a axis and a transverse spin wave lying in the basal plane. An alternative model was proposed in Ref. 33 (hereinafter denoted as a cycloid model), which describes the magnetic structure of $TbNi_5$ as the superposition of ferromagnetic moment along the a axis and a helix with a rotation plane parallel to the c axis. It is worth noting that the incommensurate structure of $TbNi_5$ can be easily destroyed by a relatively weak external magnetic field,[34] which makes it very difficult, if not impossible, to predict the correct magnetic model of $TbNi_5$-related compounds solely based on bulk magnetic measurements. Hence, it is not surprising that there is indeed controversy in the literature with regard to the magnetic states of $Tb(Ni_{1-x}Cu_x)_5$ compounds.[33,35] A collinear ferromagnetic structure was inferred in Ref. 33 from neutron-diffraction data on the compounds with $x=0.3$ and 0.4, while in Ref. 35 an incommensurate magnetic structure was proposed on the basis of magnetic results for these alloys.

The aims of this work are severalfold: to determine the magnetic structure, to map out an entire phase diagram of $Tb_xEr_{1-x}Ni_5$, and to study experimentally the concentration-induced mixing of Ising-XY anisotropies, in addition to the expected commensurate-incommensurate phase transition. For comparative studies, we have also investigated $Tb_yY_{1-y}Ni_5$ and $Y_yEr_{1-y}Ni_5$ by doping nonmagnetic Y at the rare-earth sites.

II. EXPERIMENTS

We prepared our samples: $Tb_xEr_{1-x}Ni_5$, $Tb_yY_{1-y}Ni_5$, and $Y_yEr_{1-y}Ni_5$ with $0 \leq x \leq 1.0$ and $0.3 \leq y \leq 0.7$, at the Institute of Metal Physics by the induction melting method using alumina crucible under an argon atmosphere. We used pure starting materials: Tb, Er, and Y metals of 99.9% purity and nickel of 99.99% purity. Slightly excess rare-earth metals were added to ingots in order to achieve stoichiometric compositions based on our experience. The chemical composition of the ingots was then monitored by gravimetric chemical analysis. The composition of all our samples was found to be within 2 at. % of the correct stoichiometry. All the ingots were subsequently annealed at 1100 °C under a pure helium atmosphere for 22 h followed by quenching into water. According to metallographic and x-ray analysis, all the samples formed in the single-phase $CaCu_5$-type structure. By optimizing the quenching process, we could also produce single-crystal samples of a spherical shape with 1.5 mm in diameter by cutting out large grains and treating them by means of an abrasive disk and electropolishing. The orientation of the single-crystal samples was determined by the x-ray Laue method with an accuracy better than 2°.

We performed ac-susceptibility and dc-magnetization measurements on several single crystals: $Tb_xEr_{1-x}Ni_5$ ($x=0$, 0.2, 0.3, 0.4, 0.6, 0.8, and 1.0) and $Tb_yY_{1-y}Ni_5$ as well as $Y_yEr_{1-y}Ni_5$ ($y=0.3$, 0.4, 0.5, 0.6, and 0.7). In addition, magnetization were carried out on $Tb_xEr_{1-x}Ni_5$ polycrystals with $x=0$, 0.1, and 0.925. For these measurements, we used two commercial superconducting quantum interference device (SQUID) magnetometers [Magnetic Property Measurement System (MPMS-5XL), Quantum Design, USA] with fields applied along the a and c axes at the Institute of Metal Physics and SungKyunKwan University. We also measured the specific heat of several polycrystal samples using a commercial equipment [Physical Property Measurement System (PPMS), Quantum Design, USA] at the Paul Scherrer Institut, Switzerland.

In order to study how magnetic structure changes with doping, we have also carried out neutron-powder-diffraction experiments on $Tb_xEr_{1-x}Ni_5$ ($x=0.2$, 0.3, 0.4, 0.6, 0.8, and 1.0) using the C2 high-resolution diffractometer of the NRC, Chalk River Laboratories, with $\lambda=2.37$ Å. Additional diffraction experiments have been made on powder samples with $x=0$, 0.1, and 0.925 by using the high resolution powder diffractometer (HRPD) diffractometer of the HANARO reactor at the KAERI with $\lambda=1.83$ Å. We used the Rietveld refinement program FULLPROF (Ref. 36) for the analysis.

III. EXPERIMENTAL RESULTS

A. Magnetic ground state

Figure 1 presents the experimental and calculated neutron-diffraction patterns of a few representative data. The

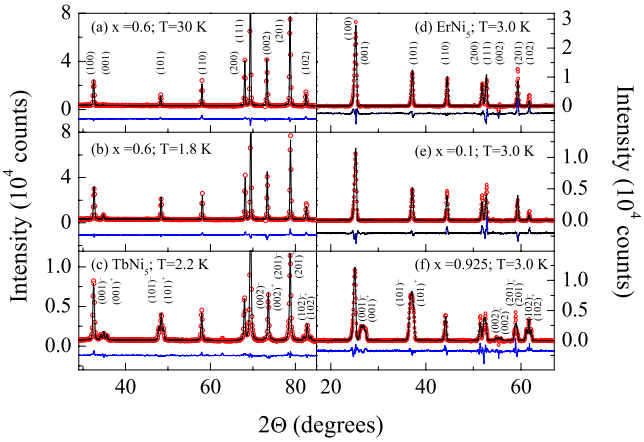

FIG. 1. (Color online) Observed (symbols) and calculated (line) neutron-diffraction patterns: (a) $Tb_{0.6}Er_{0.4}Ni_5$ at 30 K, (b) $Tb_{0.6}Er_{0.4}Ni_5$ at 1.8 K, (c) $TbNi_5$ at 2.2 K, (d) $ErNi_5$ at 3 K, (e) $Tb_{0.1}Er_{0.9}Ni_5$ at 3 K, and (f) $Tb_{0.925}Er_{0.075}Ni_5$ at 3 K. (a)–(c) show the raw data, whereas (d)–(f) show only magnetic scattering after subtracting off the nuclear contribution from the raw data as discussed in the text. Difference curves are shown at the bottom of each plot.

neutron patterns of all the $Tb_xEr_{1-x}Ni_5$ compounds taken at 30 K above T_C are almost identical since the coherent scattering lengths of Tb($b=0.74\times10^{-12}$ cm) and Er($b=0.78\times10^{-12}$ cm) are very close to each other.[37] Upon cooling below the magnetic transition temperature, however, Bragg-peak intensities increase due to the contribution from magnetic scattering. For example, the diffraction patterns of the compounds with $x\leq0.8$ at 1.8 K exhibit strong magnetic contribution to the (001) reflection, which tends to increase with x values [see Figs. 1(a) and 1(b)]. On the other hand, it becomes absent in the compositions with $x\leq0.2$ [see Figs. 1(d) and 1(e)]. Of further notice is that there are significant satellite peaks observed for $TbNi_5$ and $Tb_{0.925}Er_{0.075}Ni_5$ [see Figs. 1(c) and 1(f)], which are totally absent for all the other compositions.

Our analysis of the neutron-diffraction data demonstrate that all the $Tb_xEr_{1-x}Ni_5$ compounds form in a single phase with the hexagonal $CaCu_5$-type structure (space group $P6/mmm$): R ions at 1a position and Ni atoms at 2c and 3g positions. In Fig. 2, we summarize the concentration dependence of the a and c lattice parameters of the unit cell. As one can see, with increasing Tb concentrations the a parameter gets increased by about 0.04 Å, with very little change in the c parameter (a meager change of 0.002 Å).

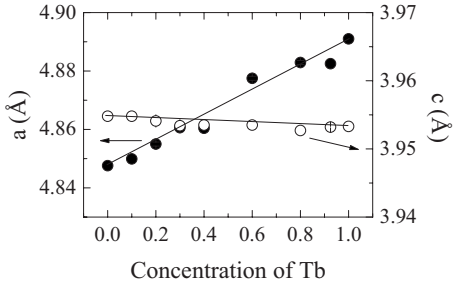

FIG. 2. Concentration dependence of the a and c lattice parameters of $Tb_xEr_{1-x}Ni_5$ determined at low temperature ~1.8–3 K with the lines following Vegard's law.

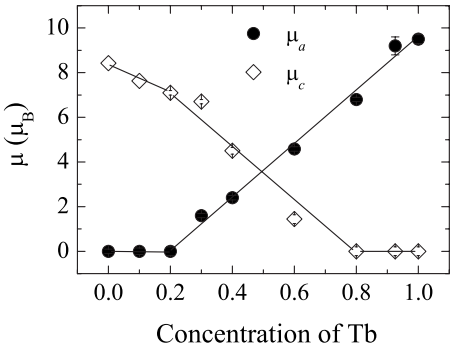

FIG. 3. Concentration dependence of the R-ion magnetic-moment components in $Tb_xEr_{1-x}Ni_5$ with the c-axis moments (μ_c) and basal plane moments (μ_a). The lines are guides for the eyes.

For $x\leq0.8$ the size of the magnetic unit cell coincides with that of the crystal unit cell, i.e., the wave vector of the magnetic structure $\mathbf{k}=0$. The aforementioned fact that the (001) peak grows in intensity with x points to the increase in a magnetic moment projected onto the basal plane. By the Rietveld refinement procedure, we obtained the a-axis (μ_a) and c-axis (μ_c) components of the R- and Ni-ion magnetic moments. In all the cases, the agreement R-factor (R_{mag}) and χ^2 quantities were better than 5% and 8%, respectively. Our analysis showed that there was a significant magnetic moment only at the R ions, while the Ni atoms were found to have much smaller moments, less than $0.2\mu_B$. Therefore, in the discussion below we ignored the Ni moment; then all the compounds with $x\leq0.8$ have ferromagnetic structures. As one can see from Fig. 3, the compounds with $x\leq0.2$ possess only μ_c, whereas concentrations $x\geq0.8$ have only μ_a. The alloys with $0.3\leq x\leq0.6$ have both in-plane and c-axis magnetic components.

Using the μ_a and μ_c values, a total magnetic moment can be calculated as $\mu_{\mathrm{tot}}=\sqrt{\mu_a^2+\mu_c^2}$ as well as its orientation with respect to the c axis with the angle of $\vartheta=\arctan(\mu_a/\mu_c)$. The obtained μ_{tot} and ϑ values are plotted in Fig. 4. It is noticeable that as shown in Fig. 4(b) the experimental data points are described reasonably well by a theoretical line based on a simple model with two (Tb and Er) orthogonal moments,

$$\mu_{\mathrm{tot}}=\{(7.3x)^2+[8.42(1-x)]^2\}^{1/2}, \quad (1)$$

where 7.3 is the Tb-ion moment in a ferromagnetic state of $TbNi_5$ measured under an external magnetic field $\mu_0H=3.5$ kOe (Ref. 33) and 8.42 is the Er-ion moment in $ErNi_5$ taken from Fig. 3. We note that the agreement becomes less satisfactory for $x\geq0.8$. This comparison then allows us to conjecture that the magnetic moments of the Tb and Er ions keep their original values over a concentration range of $0\leq x\leq0.8$.

At this point, it is necessary for us to clarify how we determined the Tb-ion magnetic moment for the compounds with $x=0.925$ and 1.0 in Fig. 3. First of all, the existence of the satellite peaks in the neutron diagrams of $TbNi_5$ and $Tb_{0.925}Er_{0.075}Ni_5$ evidences a modulated magnetic structure for these two compounds. As discussed above, two compet-

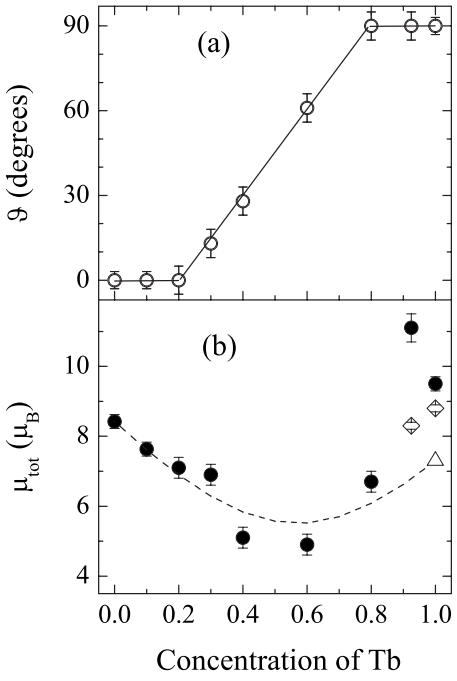

FIG. 4. Concentration dependence of (a) the angle between the total Tb-ion moment and the c axis and (b) the total magnetic moment. In (b), the open diamonds represent μ_{tot} calculated by using the cycloid model; the open triangle symbol denotes μ_{tot} in a ferromagnetic state (Ref. 33). The dashed line in (b) was calculated by using Eq. (1), while the line in (a) is a guide for the eyes.

ing magnetic models—one is the FAN-like structure and the other is the so-called cycloid model—have been proposed for the $TbNi_5$ incommensurate magnetic structure.[31–33] We note that in both models the magnetic structure is described by two wave vectors: $\mathbf{k}_1=0$ and $\mathbf{k}_2=2\pi/c(0,0,\tau)$ with $\tau=0.019$.

In the FAN-like model, Tb-ion magnetic moment has a ferromagnetic component along the a axis (μ_F) and a modulated component (μ_{mod}) like a transverse spin wave lying in the basal plane.[31,32] Using the basis functions of the irreducible representations of the space group $P6/mmm$ at the $1a$ position (please see Ref. 32 for detailed information), one can obtain the analytical form of the Tb-spin ordering in the nth cell for the FAN-like model,

$$\vec{S}_{FAN} = c_F\vec{S}(100) + c_{mod}\vec{S}(120)\cos(2\pi\tau n), \tag{2}$$

where c_F and c_{mod} are the mixing coefficients; $\vec{S}(100)$ and $\vec{S}(120)$ are the basis functions.

In the cycloid model, the modulated component rotates like magnetic moments in a simple spiral. The rotation plane is perpendicular to a ferromagnetic component,[32] which is oriented along the a axis. Then it can be easily shown that the $TbNi_5$-magnetic structure of the cycloid model can be described by the following formula:

$$\vec{S}_{cyc} = c_F\vec{S}(100) + c^1_{mod}\vec{S}(120)\cos(2\pi\tau n) + c^2_{mod}\vec{S}(001)\sin(2\pi\tau n). \tag{3}$$

Thus, in the FAN-like model, the Tb-ion moment lies in the basal plane, while in the cycloid model it possesses components in both a and c axes.

Using Eqs. (2) and (3) and the experimental neutron patterns of $TbNi_5$ taken at 2.2 K in Fig. 1(c), we obtained the following values for the Tb-ion total magnetic moment and its components: $\mu_{tot}=9.5(2)\mu_B$, $\mu_F=4.9(1)\mu_B$, and $\mu_{mod}=8.2(2)\mu_B$ for the FAN-like model; $\mu_{tot}=8.8(2)\mu_B$, $\mu_F=5.4(1)\mu_B$, and $\mu_{mod}=6.9(2)\mu_B$ for the cycloid model. Table I presents the observed and calculated intensities of the magnetic Bragg reflections and satellites. As one can see in Table I, both models produce similar values of μ_{tot}, and its orthogonal components and their R-agreement factors are also close to each other. For example, we obtained the R_{mag} factors of 4.6% and 5.8% for $TbNi_5$ with the FAN-like model and the cycloid model, respectively. In spite of the seemingly similar values of the refined results, the two models can be critically distinguished by examining directly how accurately they describe the intensity of the $(001)^-$ and $(001)^+$ satellites. The intensities of these satellites depend solely on the modulated component projected on the basal plane. As can be seen from Table I, the FAN-like model shows better agreement for the $(001)^-$ and $(001)^+$ satellites than the cycloid one.

We also used both FAN-like and cycloid models to determine the magnetic structure of $Tb_{0.925}Er_{0.075}Ni_5$ with the wave vectors of $\mathbf{k}_1=0$ and $\mathbf{k}_2=2\pi/c(0,0,0.018)$. The following values were then obtained from the analysis: $\mu_{tot}=11.1(2)\mu_B$, $\mu_F=5.4(1)\mu_B$, and $\mu_{mod}=9.7(1)\mu_B$ for the FAN-like model; $\mu_{tot}=8.3(2)\mu_B$, $\mu_F=6.7(1)\mu_B$, and $\mu_{mod}=4.8(1)\mu_B$ for the cycloid model. The intensities observed and calculated for the two models are also given in Table I. As in the case of $TbNi_5$, the most significant difference between the two models is found in the intensities of the $(001)^-$ and $(001)^+$ satellites.

B. Temperature dependence

Figure 5 shows ac susceptibility (χ) measured along the a and c axes for $x=0.3$, 0.4, and 0.6. Interestingly, for all the concentrations both $\chi(T)$ curves (a- and c-axes data) have a maximum at different temperatures. For example, the $x=0.3$ sample has the c-axis component of the Tb-ion magnetic-moment ordering at a higher temperature than that of the a-axis component. For $x=0.4$ and 0.6, an ordering of basal plane components occurs before an ordering of spin component along the c axis. It should be noted that for $x=0.4$ and 0.6, the $\chi(T)$ curves of the lower-temperature transition are equally sharp, indicative of a well-defined second-order phase transition. Similarly, in the compounds with $x=0$ and 0.2 ($x=0.8$ and 1.0), a maximum was observed only for one $\chi(T)$ curve, demonstrating that samples at both ends have quite different magnetic structures. We associate the maxima observed in the $\chi(T)$ curves with the transition temperatures, at which a long-range magnetic ordering develops with the moments aligned along either a axis or c axis. A passing comment, in this paper we only use the real part of ac susceptibility, since the imaginary part of ac susceptibility is several orders of magnitude weaker for all our samples.

For comparative studies, we also measured the susceptibility and magnetization of $Tb_yY_{1-y}Ni_5$ and $Y_yEr_{1-y}Ni_5$ al-

TABLE I. Observed and calculated intensities of the magnetic Bragg reflections and satellites for the FAN-like and cycloid models: $TbNi_5$ at 2.2 K and $Tb_{0.925}Er_{0.025}Ni_5$ at 3 K. Θ is the scattering angle, while I_{obs}, I_{FAN}, and I_{cyc} are the measured and calculated intensities for the FAN-like and cycloid models, respectively. R_{Br}, R_f, and R_{mag} are Bragg, profile, and magnetic agreement factors, respectively.

	$TbNi_5$				$Tb_{0.925}Er_{0.075}Ni_5$			
hkl	2Θ (deg)	I_{obs}	I_{FAN}	I_{cyc}	2Θ (deg)	I_{obs}	I_{FAN}	I_{cyc}
(100)	32.5	1888	1897	2257	25.1	6944	7392	7782
$(001)^-$	34.2	300	279	173	26.3	1058	1035	850
(001)	34.9	396	402	412	26.8	1178	1256	1256
$(001)^+$	35.6	227	256	158	27.3	1038	953	785
$(101)^-$	47.9	530	628	568	36.7	2584	2621	2379
(101)	48.4	1138	1194	892	37	3136	3262	2991
$(101)^+$	48.9	580	606	541	37.4	2368	2514	2243
(110)	58	492	526	612	44.1	1861	1894	2288
(200)	68	345	365	435	51.4	1263	1255	1267
$(111)^-$	69	238	236	267	52.1	886	910	958
(111)	69.5	348	350	311	52.4	1158	1175	1134
$(111)^+$	69.9	232	232	256	52.7	912	894	960
$(002)^-$	72.8	45	51	32	54.8	151	165	120
(002)	73.7	70	75	77	55.3	194	204	220
$(002)^+$	74.5	30	49	30	55.8	118	157	146
$(201)^-$	78.4	190	172	206	58.7	631	627	536
(201)	78.8	264	256	234	58.9	811	818	726
$(201)^+$	79.2	182	169	200	59.2	601	618	521
$(102)^-$	82	200	218	153	61.1	723	714	564
(102)	82.8	318	322	316	61.6	1019	882	867
$(102)^+$	83.7	166	211	147	62.1	734	682	517
R_{Br} (%)			2.9	3.2			2	7.1
R_f (%)			1.4	2.5			1.4	3.9
R_{mag} (%)			4.6	5.8			3.3	10.5

loys. By studying samples with nonmagnetic Y doped at either Tb or Er sites, we expected to have better understanding of the magnetic behavior of Tb and Er ions alone. Indeed these new alloys show more clearly how the magnetic transition of either Tb or Er ions develops with doping. What is surprising from this measurement is that for a given concentration of $Tb_xEr_{1-x}Ni_5$, the magnetic behavior of the Y-doped compounds with the same composition of Tb or Er show almost the same transition temperature with the same anisotropy. For example, as shown in Fig. 5(a) $Tb_{0.3}Y_{0.7}Ni_5$ shows a transition in the *a*-axis susceptibility at the same temperature as the *a*-axis susceptibility of $Tb_{0.3}Er_{0.7}Ni_5$, while $Y_{0.3}Er_{0.7}Ni_5$ has a peak in the *c*-axis susceptibility at the same temperature as the *c*-axis susceptibility of $Tb_{0.3}Er_{0.7}Ni_5$. We have confirmed similar behavior for several other compositions. This then—we think—constitutes a clear experimental evidence supporting our conclusion that both Tb and Er order at their own temperatures independently of each other.

As another way of checking the bulk transition temperatures, we have also measured the heat capacity of several compositions. Figure 6 presents specific heat $C_p(T)$ for $Tb_xEr_{1-x}Ni_5$. For $x=0$, 0.2, 0.8, and 1.0, $C_p(T)$ exhibits a maximum at temperatures where maxima were observed in the $\chi(T)$ data. The $C_p(T)$ shows two maxima for the compounds with $x=0.4$ and 0.6, as expected from the susceptibility measurements. In the case of $x=0.3$, the higher-temperature transition is distinctly seen, while the lower-temperature transition is difficult to discern because of its close proximity to the higher-temperature transition with a steep increase in the heat capacity due to the ordering of Er moments. Both susceptibility and heat-capacity data taken together confirm again that Tb and Er order independently.

In Fig. 7 we have summarized the doping dependence of the transition temperatures as determined from the susceptibility (Fig. 5) and heat-capacity (Fig. 6) measurements. One further salient feature in Fig. 7 is that the transition temperatures for both Tb and Er moments have almost linear concentration dependence.

The fact that Tb and Er moments order in their own easy directions independent of each other is further corroborated by the temperature-dependent neutron-diffraction data. Figure 8 shows the experimental and calculated magnetic contributions to the Bragg reflections in the neutron patterns for

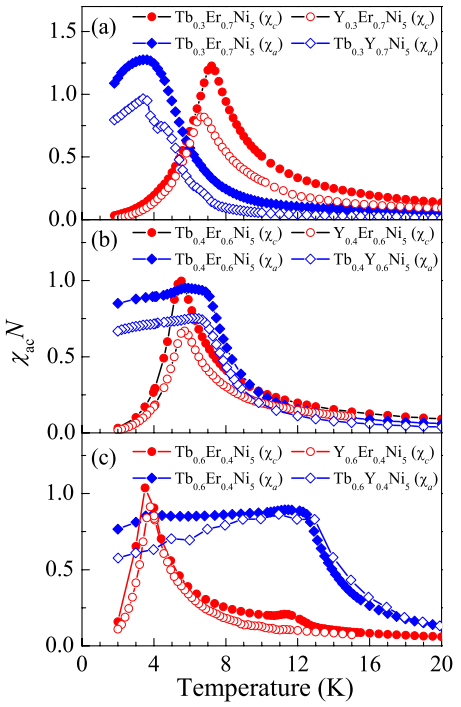

FIG. 5. (Color online) ac susceptibility $\chi(T)$ multiplied by a demagnetization factor N for several single crystals: (a) $x=0.3$, (b) $x=0.4$, and (c) $x=0.6$ of $Tb_xEr_{1-x}Ni_5$ with $H\|c$ (filled circles) and $H\|a$ (filled diamonds); $Y_yEr_{1-y}Ni_5$ with $H\|c$ (open circles) and $Tb_yY_{1-y}Ni_5$ with $H\|a$ (open diamonds) with y having the same value as x.

$x=0.6$ at various temperatures. We found that the magnetic structure of this compound can be best described by a single wave vector $\mathbf{k}=0$ at all temperatures. After ignoring the contributions from the Ni magnetic moment (our upper limit of

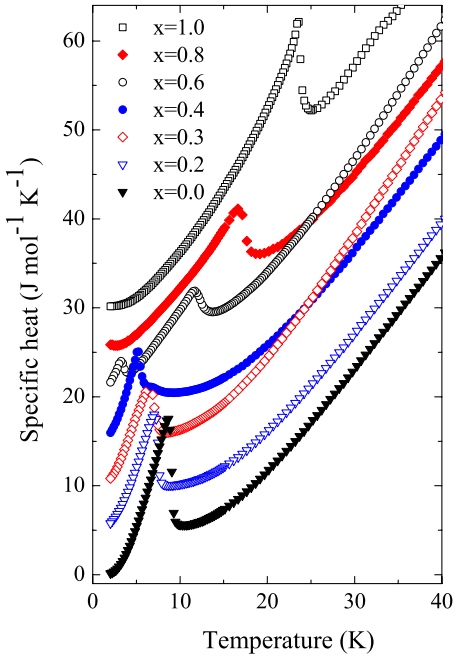

FIG. 6. (Color online) Specific heat of $Tb_xEr_{1-x}Ni_5$. For better presentation, the data are vertically shifted arbitrarily.

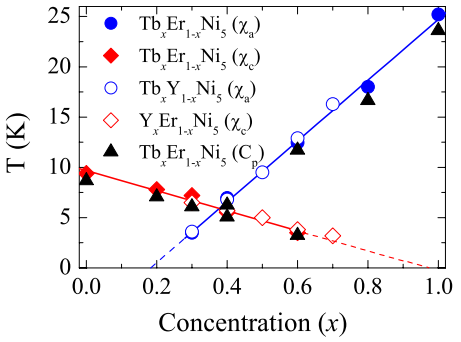

FIG. 7. (Color online) Magnetic x-T phase diagram of $Tb_xEr_{1-x}Ni_5$ obtained from ac-susceptibility and heat-capacity measurements. Curie temperatures are also plotted of $Tb_yY_{1-y}Ni_5$ (open circle) and $Y_yEr_{1-y}Ni_5$ (open diamonds). The lines are guides for the eyes.

Ni moments is $0.2\mu_B$), we determined the magnetic structure to be ferromagnetic. The temperature dependence of μ_a and μ_c obtained from the neutron patterns are given in Fig. 9(a). For comparison, the temperature dependence of μ_a and μ_c for $x=0.2$ and 0.8 are also given in Fig. 9(b). As one can see, the R-ion magnetic moment has a single component (μ_c or μ_a) for $x=0.2$ and 0.8 at all temperatures, while both components are found for $x=0.6$ at temperatures below ≈ 4 K. In this case, the single μ_a component is found to exist above 4 K before disappearing at ≈ 13 K. We emphasize that these transition temperatures determined from the neutron-diffraction data are consistent with the temperatures of the maxima found in both $\chi(T)$ and $C_p(T)$ for $x=0.6$.

Furthermore, we investigated the magnetic field dependence of magnetization. Figure 10 shows magnetization data

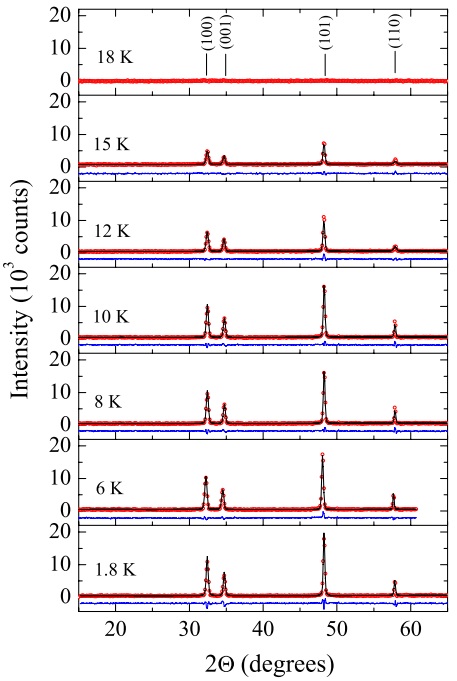

FIG. 8. (Color online) Temperature dependence of neutron data of $Tb_{0.6}Er_{0.4}Ni_5$: experimental data (symbols) and calculated patterns (line). The difference curves are shown at the bottom of each plot except for the 18 K data.

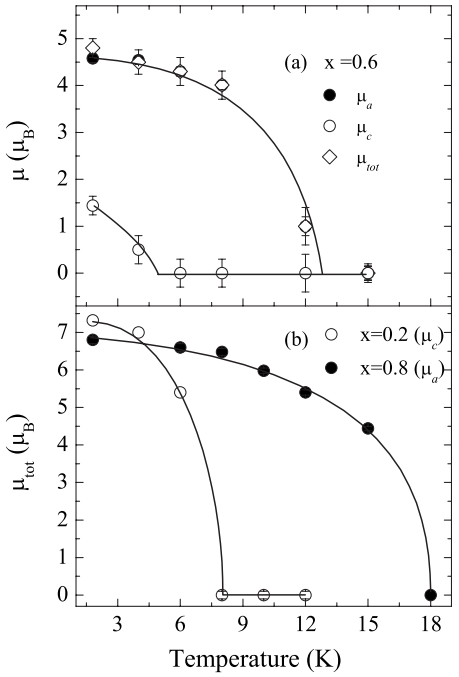

FIG. 9. Temperature dependence of total R-ion magnetic moment (μ_{tot}) and its component to the c axis (μ_c) and basal plane (μ_a) for $x=0.2$, 0.6, and 0.8 of $Tb_xEr_{1-x}Ni_5$. The lines are guides for the eyes.

for $x=0.4$ and 0.6, and $R_yY_{1-y}Ni_5$ single crystals with the corresponding compositions: $Tb_{0.4}Y_{0.6}Ni_5$, $Er_{0.4}Y_{0.6}Ni_5$, $Tb_{0.6}Y_{0.4}Ni_5$, and $Er_{0.6}Y_{0.4}Ni_5$. It can be readily seen in the figures that the spontaneous magnetic moments of $Tb_{0.4}Er_{0.6}Ni_5$ and $Tb_{0.6}Er_{0.4}Ni_5$, with field applied along and

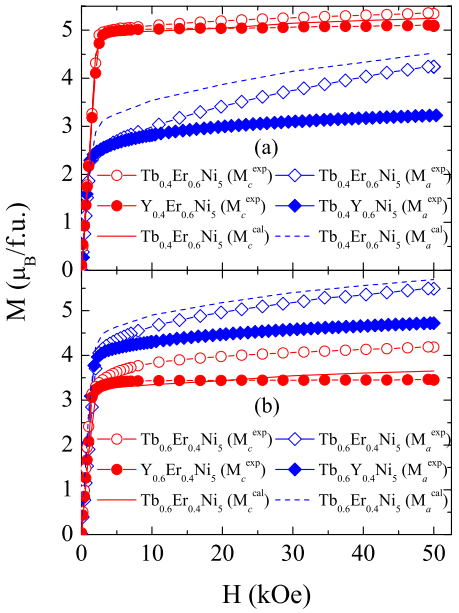

FIG. 10. (Color online) Experimental (symbols) and calculated (lines) magnetization curves of several single crystals: (a) $Tb_{0.4}Er_{0.6}Ni_5$, $Tb_{0.4}Y_{0.6}Ni_5$, and $Y_{0.4}Er_{0.6}Ni_5$; (b) $Tb_{0.6}Er_{0.4}Ni_5$, $Tb_{0.6}Y_{0.4}Ni_5$, and $Y_{0.6}Er_{0.4}Ni_5$. The circles (diamonds) are for the $c(a)$-axis data, respectively.

perpendicular to the c axis, are in good agreement with the Y-doped samples for the corresponding compositions. We used a model of two sublattices with mutually perpendicular magnetic moments[24,26] in our calculation of the magnetization curves shown in Fig. 10. Contributions of Tb and Er moments were then determined from the magnetization curves of $TbNi_5$ and $ErNi_5$ single crystals measured with field along the a and c axes.[24,26] One can see that the theoretical curves are in good agreement with the experimental data for the c axis. On the other hand, a noticeable difference seen for the a axis can be related to a possible variation in the Tb-ion magnetic moment with x when an external magnetic field is applied. In our model, we assumed that the Tb moment is constant and equal to that of a spontaneous moment of $TbNi_5$.

IV. DISCUSSION

Except for $TbNi_5$ and $Tb_{0.925}Er_{0.075}Ni_5$, all the $Tb_xEr_{1-x}Ni_5$ alloys possess a commensurate ferromagnetic structure with $\mathbf{k}=0$. Therefore, the commensurate-incommensurate phase transition occurs within a narrow concentration interval of $0.8<x<0.925$. As shown in Ref. 33, a partial substitution of Ni by Cu causes a similarly drastic change in the magnetic structure of $Tb(Ni_{1-x}Cu_x)_5$. Thus, the incommensurate structure of $TbNi_5$ is rather unstable against small external perturbations, such as magnetic field or doping, and can be easily destroyed by a partial substitution of Tb or Ni atoms.

The concentration dependencies of $\mu_a(x)$ and $\mu_c(x)$ (see Fig. 3) have approximately linear behavior for $0.2\leq x\leq 0.8$. More importantly, all our data taken together strongly suggest that the concentration dependence of $\mu_a(x)$ and $\mu_c(x)$ is *completely independent* of one another. Thus, $\mu_a(x)$ depends only on the Tb-ion content with the moment lying in the basal plane for $0.2\leq x\leq 0.8$. For the Er-ion moments, the situation is similar except that they are now parallel to the c axis. Hence, in $Tb_xEr_{1-x}Ni_5$ the Tb- and Er-ion moments are oriented along their own original directions of the easy magnetic axis because the Tb and Er ions have relatively large single-ion anisotropies, larger than exchange interactions.

One then wonders how individual Tb and Er ions interact magnetically with each other without perturbing the other. For this discussion, it is very important for us to note that the Curie temperatures of $Tb_xEr_{1-x}Ni_5$ with $H\|a$ axis coincide with those of $Tb_yY_{1-y}Ni_5$ (see Figs. 5 and 7). Similar behavior is also seen for $Y_yEr_{1-y}Ni_5$ measured with field along the c axis. These rather unusual results indicate that the exchange interaction between Tb and Er moments does not play a noticeable role in their orientations. This is also supported by the good agreement between the experimental and calculated magnetization curves obtained under the assumption of the independent arrangement of the Tb- and Er-ion magnetization along their individual easy directions (see Fig. 10). Thus, $Tb_xEr_{1-x}Ni_5$ can be considered as a good experimental example with two noninteracting order parameters. Our findings would then appear to be surprising considering the fact that the Tb and Er ions, having large moments themselves, are in close proximity in the crystal. An answer for

this puzzle comes from the following observation. Since we do not perturb the conduction band by doping, the RKKY interaction—the main source of magnetic interaction—remains intact for all the compositions. Therefore, regardless of compositions, Tb and Er interact magnetically with the other Tb and Er ions with diminished strength, which would then naturally lead to lower transition temperatures as seen in our experiment. In this regard, resistivity measurements can be a quite useful tool probing scattering of the conduction electrons by the rare-earth moments as demonstrated by some early studies.[38] In accordance with Ref. 20, one can expect that the concentration dependence of $T_C(x)$ should be smooth at a tetracritical point, at which the four different phases meet. Indeed our experimental magnetic phase diagram (see Fig. 7) appears to be consistent with this theoretical prediction too.

As mentioned before, previous studies with competing Ising-*XY* anisotropies raised questions about the lower-temperature phase boundaries. For example, some mixed systems such as Tb-Tm alloys[39] showed that the lower-temperature phase boundary is as sharp as the higher-temperature one. On the other hand, in other random mixtures, such as $Fe_{1-x}Co_xBr_2$,[19] the transition at the two lower-temperature boundaries are less sharp—much more smeared out—compared with the higher-temperature ones. According to Ref. 40, random field, arising from nondiagonal exchange interaction in such a mixture, makes the lower-temperature phase boundaries to be smeared or even to disappear. Several conclusions in Refs. 21 and 41 implied that such off-diagonal anisotropy energy [random anisotropy model (RAM)] becomes more relevant for the transition at the lower-temperature boundaries while random fields do not play a leading role. The RAM is relevant for the *XY*-like component, while the Ising-type component is not affected by RAM. According to Ref. 41 the phase diagrams shown in Fig. 7 of this paper is possible when random anisotropy is large. We think that it actually describes well what takes place in $Tb_xEr_{1-x}Ni_5$ since a main contribution to the random anisotropy originates from the single-ion anisotropies of Tb and Er.

V. CONCLUSION

In order to study the magnetic properties and to map out the entire magnetic phase diagram of $Tb_xEr_{1-x}Ni_5$, which is the ideal example of a random magnet with competing orthogonal Ising-*XY* anisotropies, we have carried out extensive studies using several experimental techniques including magnetic, heat-capacity, and neutron-diffraction measurements.

According to our studies, all the compounds (except for $TbNi_5$ and $Tb_{0.925}Er_{0.075}Ni_5$) possess a ferromagnetic structure with $\mathbf{k}=0$. It is interesting to note that the *R*-ion magnetic moments are oriented along the *c* axis in the compositions with $x \leq 0.2$, whereas they are aligned in the basal plane for $x \geq 0.8$. For the intermediate compositions ($x=0.3$, 0.4, and 0.6) we have found that the Tb-ion magnetic moments lie in the basal plane, while the Er-ion moments are parallel to the *c* axis. Thus, the Tb- and Er-ion magnetic moments order following their original magnetic easy directions. At the same time, the magnetic structures of $TbNi_5$ and $Tb_{0.925}Er_{0.075}Ni_5$ are best described by the superposition of the ferromagnetic and modulated components of the Tb-ion magnetic moment with two wave vectors: $\mathbf{k}_1=0$ and $\mathbf{k}_2=2\pi/c(0,0,\tau)$, where $\tau=0.019(1)$ and 0.018(1) are for $TbNi_5$ and $Tb_{0.925}Er_{0.075}Ni_5$, respectively.

Another interesting point is that the *concentration-temperature* (*x*-*T*) magnetic phase diagram of $Tb_xEr_{1-x}Ni_5$ shows two straight lines, intersecting at a tetracritical point. The smooth manner of $T_C(x)$ at the tetracritical point is in good agreement with the theoretical predictions of the Ising-*XY* systems with two decoupled order parameters.[20]

ACKNOWLEDGMENTS

We acknowledge K. A. McEwen for useful comments. Work at the Institute of Metal Physics was performed with supports of RAS Program (Project No. 01.2.006 13394), Quantum physics of condensed matter (Project No. 13/24), and SCOPES 2005–2008 (Grant No. IB7420-110849). Work at SungKyunKwan University was supported by the Korea Research Foundation (Grant No. KRF-2008-220-C00012), the Korea Science and Engineering Foundation (Grants No. R17-2008-033-01000-0 and No. R31-2008-000-10029-0), and the CNRF project. Experiments at the KAERI were carried out through Neutron Science 21 program. ORNL/SNS is managed by UT-Battlelle, LLC, for the U.S. Department of Energy under Contract No. DE-AC05-00OR22725.

*pirogov05@gmail.com
†jgpark@skku.edu

[1] S. Fishman and A. Aharony, Phys. Rev. B **19**, 3776 (1979).
[2] D. Mukamel, Phys. Rev. Lett. **46**, 845 (1981).
[3] P. Kettler, M. Steiner, H. Dachs, R. Germer, and B. Wanklyn, Phys. Rev. Lett. **47**, 1329 (1981).
[4] Yadin Y. Goldschmidt and A. Aharony, Phys. Rev. B **32**, 264 (1985).
[5] G. Busiello and D. I. Uzunov, Phys. Rev. B **40**, 7321 (1989).
[6] N. Douarche, F. Calvo, P. J. Jensen, and G. M. Pastor, Eur. Phys. J. D **24**, 77 (2003).
[7] D. Gignoux and D. Schmitt, Phys. Rev. B **48**, 12682 (1993).
[8] P. J. Jensen and H. Dreyssé, Phys. Rev. B **66**, 220407(R) (2002).
[9] M. Kiwi, J. Magn. Magn. Mater. **234**, 584 (2001).
[10] G. H. Rao, W. F. Liu, Q. Huang, Z. W. Ouyang, F. W. Wang, Y. G. Xiao, J. W. Lynn, and J. K. Liang, Phys. Rev. B **71**, 144430 (2005).
[11] A. I. Lukanin and M. V. Medvedev, Phys. Status Solidi B **121**, 573 (1984).
[12] P. Wong, Phys. Rev. B **34**, 1864 (1986).
[13] W. A. H. M. Vlak, M. J. van Dort, A. F. M. Arts, and H. W. de Wijn, Phys. Rev. B **38**, 11659 (1988).

[14] C. A. Ross, Annu. Rev. Mater. Res. **31**, 203 (2001).
[15] K. Katsumata, H. Yoshizawa, G. Shirane, and R. J. Birgeneau, Phys. Rev. B **31**, 316 (1985).
[16] R. M. Z. dos Santos and R. R. dos Santos, Phys. Rev. B **37**, 569 (1988).
[17] H. A. Mook, W. C. Koehler, M. B. Maple, Z. Fisk, D. C. Johnston, and L. D. Woolf, Phys. Rev. B **25**, 372 (1982).
[18] K. Katsumata, J. Tuchendler, and S. Legrand, Phys. Rev. B **30**, 1377 (1984).
[19] K. Katsumata, S. M. Shapiro, M. Matsuda, G. Shirane, and J. Tuchendler, Phys. Rev. B **46**, 14906 (1992).
[20] S. Fishman and A. Aharony, Phys. Rev. B **18**, 3507 (1978).
[21] M. Oku and H. Igarashi, Prog. Theor. Phys. **70**, 1493 (1983).
[22] K. Katsumata, H. Yoshizawa, G. Shirane, and R. J. Birgeneau, Phys. Rev. B **31**, 316 (1985).
[23] P. Wong, P. M. Horn, R. J. Birgeneau, C. R. Safinya, and G. Shirane, Phys. Rev. Lett. **45**, 1974 (1980).
[24] A. S. Ermolenko, A. V. Korolev, and A. G. Kuchin, Phys. Met. Metallogr. **57**, 70 (1984).
[25] A. G. Kuchin, A. V. Korolev, and A. S. Ermolenko, Phys. Met. Metallogr. **59**, 73 (1985).
[26] A. G. Kuchin and A. S. Ermolenko, Phys. Met. Metallogr. **70**, 55 (1990).
[27] N. I. Kourov, A. G. Kuchin, and A. S. Ermolenko, Phys. Met. Metallogr. **71**, 59 (1991).
[28] P. A. Algarabel, L. Morellon, M. R. Ibarra, D. Schmitt, D. Gignoux, and A. Tari, J. Appl. Phys. **73**, 6054 (1993).
[29] A. Aubert, D. Gignoux, B. Hennion, B. Michelutti, and A. Nait-Saada, Solid State Commun. **37**, 741 (1981).
[30] F. E. Kayzel, J. J. M. Franse, and R. J. Radwanski, IEEE Trans. Magn. **30**, 890 (1994).
[31] S. Lee, A. N. Pirogov, J.-G. Park, I. P. Swainson, Yu. A. Dorofeev, A. E. Teplykh, A. S. Ermolenko, E. G. Gerasimov, and A. A. Podlesnyak, Europhys. Lett. **62**, 350 (2003).
[32] A. P. Vokhmyanin, S. Lee, K.-H. Jang, A. A. Podlesnyak, L. Keller, K. Prokeš, V. V. Sikolenko, J.-G. Park, Yu. N. Skryabin, and A. N. Pirogov, J. Magn. Magn. Mater. **300**, e411 (2006).
[33] R. Lizarraga, A. Bergman, T. Björkman, H.-P. Liu, Y. Andersson, T. Gustafsson, A. G. Kuchin, A. S. Ermolenko, L. Nordström, and O. Eriksson, Phys. Rev. B **74**, 094419 (2006).
[34] S. Lee, A. A. Podlesnyak, K. Prokeš, E. V. Sikolenko, S. Ermolenko, E. G. Gerasimov, Yu. A. Dorofeev, A. P. Vokhmyanin, J.-G. Park, and A. N. Pirogov, JETP Lett. **82**, 34 (2005).
[35] V. M. T. S. Barthem, E. A. Moreira da Gama, and A. Y. Takeuchi, J. Magn. Magn. Mater. **177-181**, 1065 (1998).
[36] J. Rodríguez-Carvajal, Physica B **192**, 55 (1993).
[37] V. F. Sears, Neutron News **3**, 26 (1992).
[38] J. A. Blanco, D. Gignoux, D. Schmit, A. Tari, and F. Y. Zhang, J. Phys.: Condens. Matter **6**, 4335 (1994).
[39] P. Hansen and B. Lebech, J. Phys. F: Met. Phys. **6**, 2179 (1976).
[40] P. Wong, P. M. Horn, R. J. Birgeneau, and G. Shirane, Phys. Rev. B **27**, 428 (1983).
[41] D. Mukamel and G. Grinstein, Phys. Rev. B **25**, 381 (1982).